# Surface and Bulk Stabilization of Silicon Anodes with Mixed-Multivalent Additives: $Ca(TFSI)_2$ and $Mg(TFSI)_2$

Sohyun Park, Haoyu Liu, Joseph Quinn, Saul H. Lapidus, Yunya Zhang, Stephen E. Trask, Chongmin Wang, Baris Key, and Fulya Dogan*

**ABSTRACT:** Silicon is drawing attention as an emerging anode material for the next generation of lithium-ion batteries due to its higher capacity compared with commercial graphite. However, silicon anions formed during lithiation are highly reactive with binder and electrolyte components, creating an unstable SEI layer and limiting the calendar life of silicon anodes. The reactivity of lithium silicide and the formation of an unstable SEI layer are mitigated by utilizing a mixture of Ca and Mg multivalent cations as an electrolyte additive for Si anodes to improve their calendar life. The effect of mixed salts on the bulk and surface of the silicon anodes was studied by multiple structural characterization techniques. Ca and Mg ions in the electrolyte formed relatively thermodynamically stable quaternary Li−Ca−Mg−Si Zintl phases in an in situ fashion and a more stable and denser SEI layer on the Si particles. These in turn protect silicon particles against side reactions with electrolytes in a coin cell. The full cell with the mixed cation electrolyte demonstrates enhanced calendar life performance with lower measured current and current leakage in comparison to that of the baseline electrolyte due to reduced side reactions. Electron microscopy, HR-XRD, and solid-state NMR results showed that electrodes with mixed cations tended to have less cracking on the electrode surface, and the presence of mixed cations enhances cation migration and formation of quaternary Zintl phases stabilizing the bulk and forming a more stable SEI in comparison to baseline electrolyte and electrolyte with single multivalent cations.

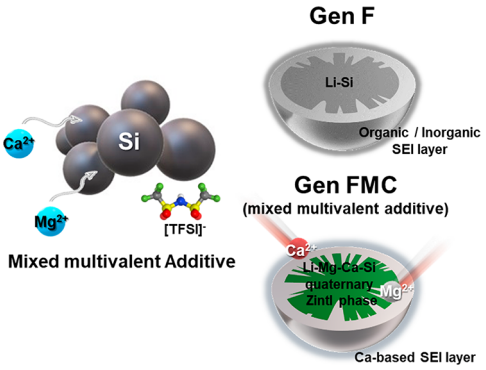


**KEYWORDS:** *Si anodes, lithium-ion batteries, calendar life, electrolyte additives, mixed-salt electrolyte*

## 1. INTRODUCTION

With the world's acute environmental issues like air pollution and oil depletion, demand for electric energy storage has increased, and lithium-ion batteries have been widely commercialized for rechargeable batteries exhibiting high energy and power density.[1,2] Currently, the application range of secondary batteries is expanding to electric vehicles and advanced energy storage systems, beyond the small-sized batteries used as the main power sources for portable electronic devices.[3] Particularly, the recent EV market is on the rise, and accordingly, electric vehicles capable of long range and fast charging are required.[4,5] Graphite is the dominant anode material in commercial LIBs for EVs. However, graphite has a limited Li storage capacity of about 375 mA h $g^{-1}$ to deliver capacity from six carbons that can intercalate one lithium ion to form $LiC_6$ during charge−discharge.[6,7] For this reason, graphite may have limited use in future energy storage applications, such as electric vehicles (EVs) and large backup power supplies. Problems such as short-range, long charging time, battery life, and output power of electric vehicles can be solved by developing high-performance anode materials to improve the battery capacity. Silicon has been considered as one of the most attractive anode materials compared to graphite due to its volumetric capacity and high gravimetric capacity (3579 mA h $g^{-1}$)[8,9] accommodating more lithium per silicon, forming a $Li_{15}Si_4$ Zintl phase at high lithiated state at 10 mV. The Si anode has a relatively lower electrochemical potential (<0.2 V vs $Li^+/Li$), leading to a high energy density from high working voltage with full cell.[10,11] However, the system still has several challenges to be resolved for high silicon concentration commercial battery applications. During lithiation, Si forms several different intermediate $Li_xSi_y$ Zintl phases that are highly reactive.[12,13] $Li_xSi_y$ phases can react with binder or electrolyte components, which can cause degradation and decomposition of the electrolytes, resulting in an unstable solid electrolyte interphase (SEI) layer and side reactions.[13−16] Formation and decomposition of $Li_xSi_y$ can also cause mechanical stress on the silicon anode, leading to cracking and degradation of Si, which can reduce electrochemical

performance. In this process, Si anode undergoes dramatic volume expansion of more than three times when charging silicon.[17,18] Volume expansion of Si can cause breakage or breaking into small pieces like pulverization of Si particles, and continuous growth of the instability of the solid electrolyte interphase layer with high resistance degrades battery performance. High electrical resistance can reduce the efficiency of cycling with a higher voltage drop across the anode. This can result in a decrease not only in the overall energy density of the battery but also a shorter lifespan. The continuous growth of the SEI layer can make the limited surface area accessible between Si and electrolyte and electrolyte decomposition and lithium consumption. Various attempts such as structural modification and formation of the SEI layer have been made to tackle this problem.

In particular, these characteristics greatly affect the performance of the battery. Calendar life is of great significance, given that battery systems are anticipated to have a lifespan of around a decade to remain a viable energy storage solution for the next generation of vehicles. In a battery system, calendar aging is caused from the formation of a passivation layer on the anode electrode and loss of Li ions to the SEI layer on the anode surface. These reactions result from anode reactions, involving electrolyte reduction and leading to SEI layer growth; cathode reactions, encompassing electrolyte oxidation and transition metal dissolution; and coupled reactions, where transition metals dissolved from the cathode impact SEI layer growth at the anode.[19] The cycle performance is also closely related to the SEI layer, as a stable SEI is essential to provide extended charge−discharge cycles for Si anodes to protect electrolytes from continuous degradation and the resulting depletion. Electrolyte design is the typical approach not only to build up a high-quality SEI layer but also for structure modification with solvation structure in the bulk, which is significant and is beneficial for the enhanced electrochemical performance of the Si anode.

In our previous reports, we introduced incorporating multivalent salts into the electrolyte as a means of stabilizing silicon anions by forming more stable Li−M−Si ternaries that improve both cycling life and form more stable SEI on the Si surface, improving calendar life performance.[20] Multivalent salts (including $Mg(TFSI)_2$ and $Ca(TFSI)_2$) in the electrolyte were found to promote formation of Li−M−S (M = Mg and Ca) ternary Zintl phases during the first lithiation process, which improves lithiation/delithiation stability and reduces area-specific impedance. These multivalent cations not only can form ternary phases (Li−Ca/Mg−Si) but also react with F ion in the electrolyte to from passivating metal fluorides ($MgF_2$/$CaF_2$) contained in the inorganic SEI layer on silicon particles, stabilizing the SEI.[21] The resulting SEI layer proved to be protective of the silicon particles from side reactions, leading to enhance calendar life performance.[22]

In this study, we introduce a new approach for the application of multivalent salts as mixed additives containing $Mg(TFSI)_2$ and $Ca(TFSI)_2$ for Si anodes in lithium-ion batteries.[21,23] Previous research has explored the use of various multivalent salts as single additives in electrolytes.[21,24] The new approach involves utilizing Mg cation insertion into the bulk to form a Li−M−Si Zintl phase for stabilizing the bulk Zintl phase, while Ca cations primarily stabilize the surface with $CaF_2$ in the SEI layer protecting the silicon surface during lithiation and delithiation. Rietveld refinement analysis with synchrotron XRD confirmed that the use of mixed additives promoted the total metal insertion into the bulk as opposed to single cation use, forming Li−M−Si quaternary phases in the bulk, while NMR and cryo-TEM imaging revealed the formation of a more stable SEI layer on the surface compared to a baseline electrolyte system. By combining the beneficial features of both salts, a synergistic effect was observed which improved the battery's calendar life performance, cycle performance, and Coulombic efficiency.

## 2. EXPERIMENTAL SECTION

**2.1. Electrode and Electrolyte Preparation.** All electrodes were provided by CAMP (Argonne's Cell Analysis, Modeling, and Prototyping) facility. The Paraclete Si electrode slurry is composed of 80 wt % Si material which was produced by Paraclete Energy (Chelsea, MI), 10 wt % hard carbon (C45), and 10 wt % lithium polyacrylate (LiPAA) binder mixture with deionized water coated on Cu foil. The coating loading of active materials is around 0.98 mg/cm$^2$ with 10 $\mu$m as the coating thickness. The ORNL Si was prepared by Oak Ridge National Laboratory (ORNL) from high-energy milling of Si boules using a Zoz-Simoloyer CM01 mill.[25] The ORNL Si electrode is composed of 80 wt % ORNL Si, 10 wt % hard carbon (C45), and 10 wt % P84 polyimide (NMP) by Ensinger, with a coating loading of active materials of around 1.19 mg/cm$^2$ and a thickness of 14 $\mu$m.

The cathode electrodes were prepared by using two different materials: NMC 532 and NMC 811. The NMC 532 cathode electrode was made by mixing 90 wt % NMC 523, 5 wt % hard carbon (C45), and 5 wt % PVDF binder (Solvey 5130). The resulting mixture was then laminated onto aluminum foil. The NMC 811 electrode was prepared with the same ratio as NMC 532 but with NMC 811 materials from TARGRAY.

The Si electrode was punched into 15 mm diameter, and the cathode electrode was punched into a 14 mm diameter considering the N/P ratio. For the baseline electrolyte (Gen F), we used 1.2 M $LiPF_6$ in ethylene carbonate (EC) and ethyl methyl carbonate (EMC) in a 3:7 volume ratio, with 3 wt % fluoroethylene carbonate (FEC). To produce a mixed-salt electrolyte, Mg and Ca salts with a purity of 99.5% were purchased from the Solvionic company. Both salts were dried at 150 °C under vacuum overnight in a glovebox, and 0.03 M $Mg(TFSI)_2$ and 0.07 M $Ca(TFSI)_2$ were dissolved in the Gen F electrolyte to create the mixed additive electrolyte (Gen FMC).

**2.2. Electrochemical Performance Analysis.** The full cells were assembled using a 2032-coin type cell in an Ar-filled glovebox. Galvanostatic charge/discharge tests were performed on coin cells within the voltage range 3.0−4.1 V to assess both calendar and cycle performance, utilizing a MACCOR battery test system. The Si/NMC532 full cells were activated using 3 cycles at a $C/20$ rate for formation, following a 4 h OCV rest period. The cells were then kept at 4.1 V for one month, followed by two diagnostic cycles at a $C/20$ rate. The cyclic performance of the Si/NMC532 full cells was tested at a $C/20$ rate for 3 cycles during formation and then at a $C/3$ rate for 100 cycles. Electrochemical impedance spectroscopy (EIS) was measured in a frequency range of 100 kHz to 100 mHz during the calendar life test using the Biologic VSP potentiostat model (VSP-300).

**2.3. Characterization of Materials.** The SEM samples were harvested from cycle and calendar life cells. The Si anode was removed from the coin cell and rinsed in 5 mL of DMC solvent for 30 s before being cut into pieces. The pieces of the electrode were then imaged using a scanning electron microscope (JEOL JSM-6610LV) equipped with an energy-dispersive spectroscopy (EDS) instrument and operated at 20 kV.

MAS NMR experiments were performed at 7.02 T (300 MHz) on a Bruker Avance III HD spectrometer using a 3.2 mm MAS probe. $^1$H spectra were acquired at 60 kHz at a constant temperature of 283 ± 0.1 K with a rotor synchronized echo pulse sequence (90°-$\tau$-180°-$\tau$-acq), where $\tau = 1/\nu r$. A $\pi/2$ pulse width of 2.5 $\mu$s was used with a sufficiently long pulse recycle delay of 15 s. The spectra were referenced to tetramethylsilane at 0 ppm. $^7$Li spectra were acquired at

60 kHz at a constant temperature of 283 ± 0.1 K with a rotor-synchronized echo pulse sequence (90°-$\tau$-180°-$\tau$-acq), where $\tau = 1/\nu r$. A $\pi/2$ pulse width of 2.5 $\mu$s was used with sufficiently long pulse recycle delays of 15 s. The spectra were referenced to a 1 M LiCl aqueous solution at 0 ppm. $^{19}$F spectra were acquired at 35 kHz at a constant temperature of 283 ± 0.1 K with a rotor synchronized echo pulse sequence (90°-$\tau$-180°-$\tau$-acq), where $\tau = 1/\nu r$. A $\pi/2$ pulse width of 2.5 $\mu$s was used with sufficiently long pulse recycle delays of 30 s. The spectra were referenced to hexafluorobenzene at 0 ppm. $^{29}$Si spectra were acquired at 20 kHz at a constant temperature of 283 ± 0.1 K with a single pulse, spin/Hahn echo, and $^{1}$H → $^{29}$Si cross-polarization (CP) measurement, with $\pi/2$ pulse width of 5 $\mu$s and various pulse/recycle delays to reflect different relaxation behaviors in Si species. The spectra were referenced to tetramethylsilane at 0 ppm. The $^{1}$H → $^{13}$C CP spectra were acquired at 20 kHz and at a constant temperature of 283 ± 0.1 K. A contact time of 4 ms was applied to both CP measurements to ensure enough spin polarization from $^{1}$H to $^{13}$C/$^{29}$Si.

Loose powder cells were utilized for ex situ XRD analysis to maximize sample loading. The cells were prepared by mixing silicon powder and hard carbon (C45) in a 1:1 weight ratio and then depositing the mixture via a slurry with acetone onto the current collector which when dried is self-supporting. To achieve full lithiation of Si, the loose powder cell was discharged to 0.05 V using a $C/100$ rate. The freshly lithiated electrode samples were then loaded into Kapton capillaries, packed with glass fiber, and sealed with epoxy inside an Ar-filled glovebox. High-resolution X-ray diffraction measurements were conducted using a Si(111) double crystal as a monochromator, at beamline 11-BM of the Advanced Photon Source. Rietveld refinements were performed by using the FullProf program.

To prepare the Cryo-STEM samples, the Si coin cells were disassembled in a glovebox filled with Ar gas. After disassembling the Si coin cells in a glovebox filled with Ar gas, the cells underwent a thorough washing process in EMC. This process effectively removed any residual electrolyte and salt, and the cells were subsequently dried under vacuum to ensure the complete removal of any moisture. After that, the cycled Si anodes were scratched with glass slides and pressed onto a Cu TEM grid. The TEM grid holder was sealed and subsequently transferred to a Gatan Cryo-Transfer Station. The sample grid was loaded onto a Gatan ELSA 696 cryo-holder using a nitrogen gas head to minimize oxygen exposure. The cryo-holder was then transferred to the STEM instrument for characterization. The samples were examined by using a 300 kV FEI Titan monochromated scanning TEM instrument with a probe aberration corrector.

## 3. RESULTS AND DISCUSSION

### 3.1. Electrochemical Performance and Impedance.

Silicon anodes with mixed multivalent cation added electrolytes were first tested in a half-cell configuration and compared with baseline electrolyte (Gen F). Table 1 provides a comprehensive list of the electrolyte formulations used in the study. The benefits of individual Ca and Mg salts as additives were covered in our previous studies,[21] and their comparison with our new mixed-salt formation on silicon calendar life is presented in Figure S1. It should be noted that the final ratio of the mixed salts used in the electrolyte was based on electrochemical test results with different electrolytes varying the cation ratios (Figure S2).

**Table 1. Electrolyte Formation and Name for Each Electrolyte Uesd in This Study**

| Electrolyte | Formulations |
|---|---|
| Gen 2 | 1.2 M $LiPF_6$ in a 3:7 mixture of EC and EMC |
| Gen F (baseline) | Gen 2 electrolyte + 3 wt % FEC |
| Gen FMC | Gen F electrolyte + 0.03 M $Mg(TFSI)_2$ + 0.07 M $Ca(TFSI)_2$ |
| Gen FM | Gen F electrolyte + 0.1 M $Mg(TFSI)_2$ |
| Gen FC | Gen F electrolyte + 0.1 M $Ca(TFSI)_2$ |

As shown in Figure S3, both the baseline Gen F and the Gen FMC electrolytes delivered an initial capacity of over 3000 mA h g$^{-1}$, approaching the theoretical capacity. However, during cycling, the capacity fade was observed to get worse in the baseline Gen F electrolyte. During the three formation cycles at $C/20$, the baseline Gen F electrolyte exhibited a capacity loss of around 687 mA h g$^{-1}$, compared to the capacity loss of the Gen FMC electrolyte (290 mA h g$^{-1}$), whereas the capacity of the Gen FMC electrolyte decreased from 2707 to 2049 mA h g$^{-1}$ during the subsequent fast cycling at $C/3$. Additionally, Figure S3b shows that the baseline Gen F electrolyte had a lower Coulombic efficiency of 95% compared to that of the Gen FMC electrolyte. For the next step, the calendar and cycle life performances of full cells with baseline and multivalent cation electrolytes were tested with the NMC 532 cathode. As shown in Figure 1, the calendar life test was started with three cycles for formation to activate the electrode with electrolyte, and then the voltage was held at 4.1 V, ending with three cycles (diagnostic) at $C/20$. During the voltage holding step, Si might undergo reversible lithiation to Si and an irreversible electrochemical reaction, related to SEI formation and concomitant $Li^+$ consumption. Figure 1b is calendar life performance data, which shows measured current response from parasitic reactions versus time during the voltage hold. The measured current serves as an indicator of current leakage and the rate of side reactions between lithiated silicon and cell components such as electrolyte and/or binder.[21] While the voltage is held at the end of the charge, irreversible side reactions can take place on the surface of the Si anode, which is measured by the current. As illustrated in Figure 1b, the Gen FMC cell exhibits lower current leakage and more converged current compared to the Gen F cell. This finding suggests that the Gen FMC cell experiences fewer irreversible side reactions, indicating a more stable SEI layer. Figure 1c visually exhibits capacity decay associated with Li intercalation to the Si anode. Compared to the Gen F cell, the Gen FMC cell has low-capacity decay during the voltage hold, suggesting the Gen F sample undergoes severe $Li^+$ consumption to the SEI or with side reactions, reflected in loss of reversible capacity. This phenomenon can also be seen in the graph of capacity change. The variation in the capacity during voltage holding is shown in Figure 1d. It is observed that a change in capacity occurs while the voltage is held, which is proportional to the side reactions and relative to the capacity at the start of the initial holding period.[26] The Gen FMC sample shows not only a capacity decay of 14%, which is less than that of baseline Gen F, but also a flattened capacity exchange curve (Figure 1d). In order to study the effectiveness of mixed-salt additives on different silicon types and surfaces, calendar life tests were also conducted at ORNL silicon (Figure S4). Consistent with the results for paraclete Si, Gen FMC showed lower current leakage than Gen F. After one month of voltage holding, Gen FMC not only exhibited lower parasitic current but also a flattened curve profile corresponding to capacity exchange. As expected, the mixed-salt electrolytes were found to be effective in improving the calendar life of the Si anode, including those of different silicon composition.

After the calendar life test of one month, ex situ SEM was carried out to confirm the surface stress of Si electrodes. The disassembled electrodes were washed with a diethyl carbonate (DEC) solvent for a few seconds to remove residual

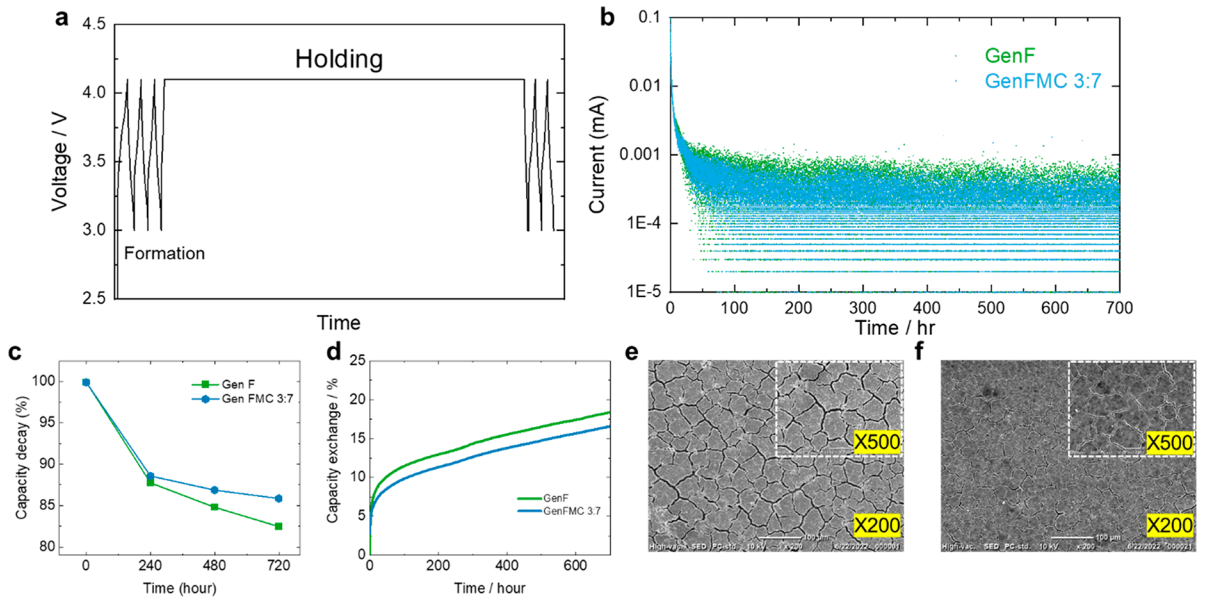


**Figure 1.** (a) Protocol curve of calendar life. (b) Current leakage of GenF and GenFMC for 1 month holding at 4.1 V. (c) Capacity decay percentage. (d) Capacity exchange based on starting to hold capacity of GenF and Gen FMC with Paraclete Si anode and NCM 532 cathode. Ex situ SEM image of (e) GenF cell and (f) Gen FMC cell after voltage holding at 4.1 V for 720 h, taken at 200× magnification. (Inset) High-magnification view (500×).

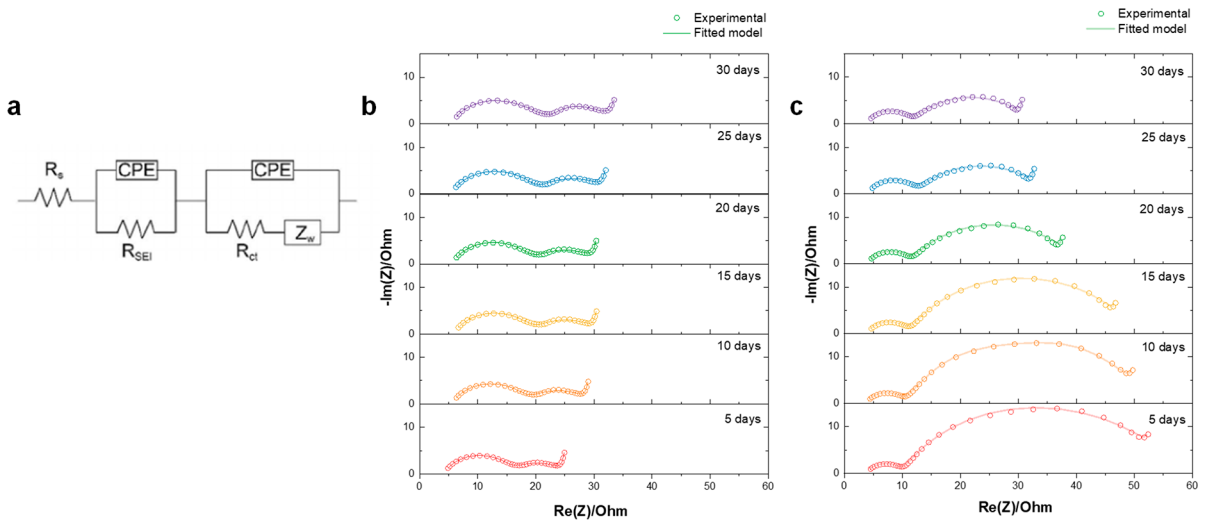


**Figure 2.** (a) Equivalent circuit model for Nyquist plot analysis and impedance spectra change of cells with (b) Gen F electrolyte and (c) Gen FMC electrolyte at 5-day intervals.

electrolytes on the surface. After washing, the Gen F electrode showed delamination from the current collector, which is shown in Figure S5. In contrast, the Gen FMC electrode remained intact and did not show any signs of delamination. As seen in SEM images, Gen F has conspicuous cracks and fractures which are distributed on the surface of the electrode; in comparison, the Gen FMC cell shows less cracking on the surface (Figure 1e,f). The observed cracking and delamination could potentially reduce the electrode's performance and cycle life as an unstable SEI layer can result in unexpected exposure of the active materials within the electrode to the electrolyte, a phenomenon predominantly attributed to particle-level fractures. This includes fractures of individual active particles and adhesive debonding between these particles and the CA/binder compound. Consequently, this situation may establish pathways for increased exposure of the active material to the electrolyte, leading to undesired chemical reactions and electrode degradation.[27] The mixed salt used in the electrolyte resulted in the formation of a stable SEI layer, which improved the surface stability and prevented cracks on the electrode surface. These findings are consistent with our previous reports, which suggested that the formation of the SEI layer, facilitated by the Ca and Mg salt, may contribute to playing a role as a buffer parasitic reaction on the surface and thus prevent cracking.[20,21]

Our cryo-STEM and solid-state NMR experiments provide a more detailed explanation of the properties of the SEI layer and surfaces, which will be discussed in the following section.

The use of the mixed-salt electrolyte also contributed to the improvement of the cycle performance, as shown in Figure S6. Cycle performance was conducted with 3 cycles of formation at C/20 and 97 cycles at C/10. During the formation step, Gen

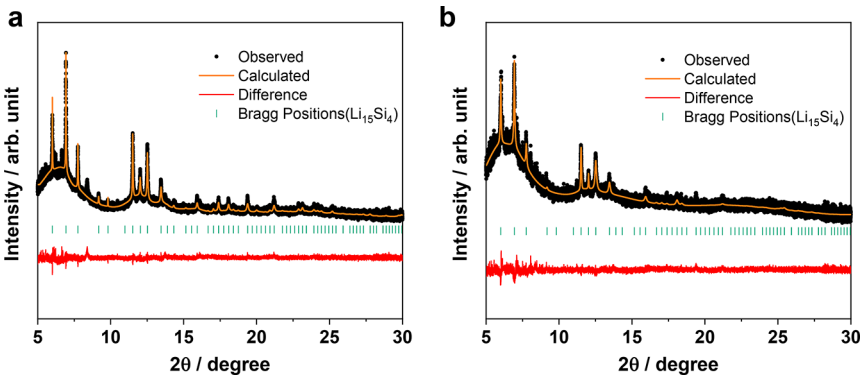


**Figure 3.** Rietveld refinement pattern for powder XRD data for (a) Gen F and (b) Gen FMC.

FMC delivered lower capacity and Coulombic efficiency than those of Gen F cell. This can be attributed to the significant influence of SEI formation and growth on Coulombic efficiency corresponding to the reaction of Si anode with mixed-salt electrolyte.[28] After 100 cycles, Gen FMC exhibits a lower capacity decay of 50% compared to that of Gen F, which shows a capacity decay of 38%. Furthermore, Gen FMC demonstrates a higher average Coulombic efficiency throughout the 100 cycles. Even after 100 cycles (Figure S7), the surface of the Gen FMC electrode shows minimal cracking due to the formation of a stable SEI layer and/or stabilized surface, similar to that observed in the calendar life test. The composition of the surface layer is studied by solid-state NMR and will be discussed in the next sections.

To investigate the resistance phenomena, EIS measurements (as shown in Figure 2) were carried out while holding a constant voltage, with measurements taken every fifth day. EIS signals reveal the various resistances present in a coin cell, including the electrolyte resistance, intrinsic resistance of the active material, and interfacial contact resistance between the electrodes and current collectors.[29] Figure 2a shows the equivalent circuit models to simulate the impedance spectra. The first resistance $R_S$ is dominated by inductive phenomena arising from the impedance measurement environment and represents the internal resistance value of the bulk materials in a battery, such as the current collector, electrolyte, and separator.[30] The high-frequency range in the impedance spectrum reflects surface resistance phenomena, which are related to the resistance of the SEI layer ($R_{SEI}$). The $R_{SEI}$ is the impedance of a layer that forms at the interface between the electrode and electrolyte, and it is attributed to the transport of $Li^+$ ions through compact ionic phases within the SEI.[31,32] The charge transfer resistance ($R_{ct}$) is visible in the lower-frequency region and represents the resistance associated with not only the transfer of charge between the electrode and electrolyte interfaces but also the diffusion of $Li^+$ ions at the outermost layer of the SEI. These two resistances ($R_{SEI}$ and $R_{ct}$) comprise the overall Li−electrolyte interfacial resistance, which can be combined as a charge-driven resistance across all interfaces.[33] While holding the voltage, the bulk resistance of Gen F gradually increased over time (from 4.1 Ω at 5 days to 5.4 Ω at 30 days), whereas the bulk resistance of Gen FMC remained relatively constant (3.8 Ω at 5 days and 3.8 Ω at 30 days) (Table S2). Additionally, Gen FMC exhibited a lower overall resistance than Gen F. Although this bulk resistance may not change significantly with the state of charge, it can be affected by factors such as electrolyte depletion and microcrack formation in the particles over time.[34] Therefore, it is possible that a side reaction occurred inside the Gen F coin cell that generated resistance. After holding for the first 5 days, Gen FMC has a semicircle that is larger than that of Gen F. The initial resistance is large because the current flow or charge transfer and diffusion are temporarily slow due to the formation of the SEI layer, but this is alleviated over time. This result is in the same vein as the reason for the low initial Coulombic efficiency of the cycle performance. This phenomenon might be caused by formation of a more complex SEI layer on the surface from mixed additives, which can increase resistance to the charge transfer at the beginning of voltage holding. Initially, the Ca and Mg additives can promote the formation of an additional SEI layer such as metal fluorides and oxides around the silicon particles. The formation of the SEI layer predominantly occurs at the beginning of the electrochemical reaction, and its growth continues slowly over subsequent cycles until it reaches a fully developed state.[28] Even though charge transfer resistance seems to be a large value at the first stage, it can be seen that the semicircle is gradually decreased through holding time. Charge transfer resistance can be influenced by factors such as the surface area of the electrode, presence of cracks, and the state of charge. As shown in Figure 1, in the case of Gen F, electrode cracking became severe after the calendar life test. This could have reduced the effective surface area of the electrode, limiting the interaction area between lithium ions and the electrolyte, and subsequently reducing the charge transfer efficiency. Another possibility is self-discharge with the cell, which can change the state of charge during long voltage hold. The semicircle representing the SEI resistance is constant during the voltage holding, which indicates that a stable SEI layer is formed without continuous chemical and/or structural evolution of the native SEI. On the other hand, the Gen F cells show steady increase over the same time frame. Especially, the SEI resistance value of Gen F has a wider increased range from 11.35 to 15.4 Ω in comparison to that of Gen FMC (6.1 to 7.68 Ω) with voltage holding time. Growth of SEI resistance might be associated with the increase in thickness of the SEI layer or change in components of the SEI layer.

**3.2. Formation of Quaternary Zintl Phases and Multivalent Cation Insertion.** The in situ formation of Li−M−Si ternary and/or quaternary Zintl phases during initial lithitation was investigated using synchrotron powder XRD with fully lithiated samples at the end of discharge. The differences between Gen F and Gen FMC electrolytes were studied separately and are shown in Figure 3. The results of the

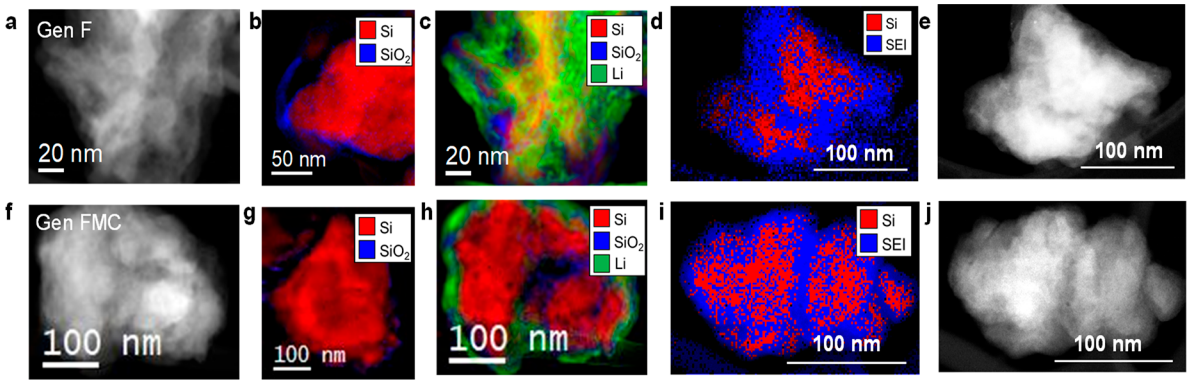


**Figure 4.** Cyro STEM, EELS, and EDS mapping analysis of Si particle with Gen F and Gen FMC after 100 cycles. (a) STEM image, (b) EELS map with Si composition, (c) Si and Li chemical mapping using MLLS models, (d) EDS mapping with Si and SEI layer, and (e) STEM image corresponding EDS mapping of Gen FM electrolyte. (f) STEM image, (g) EELS map with Si composition, (h) Si and Li chemical mapping using MLLS models, (i) EDS mapping with Si and SEI layer, and (j) STEM image corresponding EDS mapping of Gen FM electrolyte.

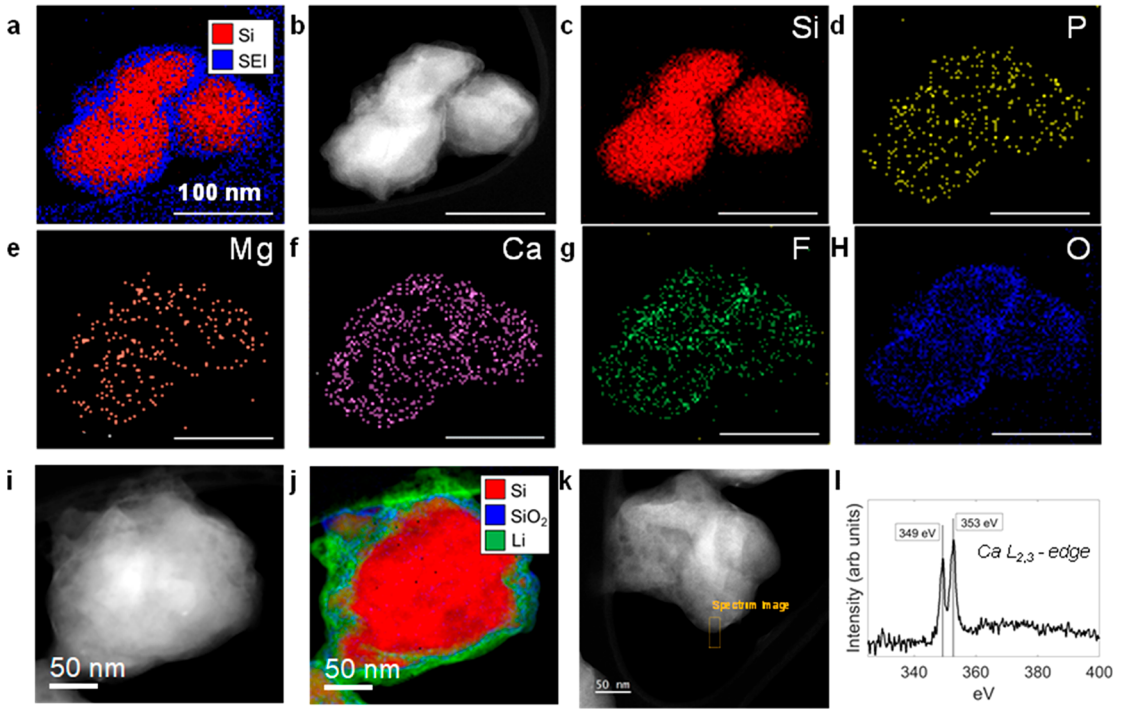


**Figure 5.** Cryo-STEM images, EELS, and EDS maps for a Si anode after calendar aging(1-month holding) with a Gen FMC electrolyte. (a) EDS maps of Si and SEI components, (b) STEM HAADF image corresponding to the EDS elemental maps, EDS elemental maps of (c) Si, (d) P, (e) Mg, (f) Ca, (g) F, (h) and O elements, (i) STEM image corresponding to EELS maps, (j) EELS maps of Li, Si, and $SiO_2$, (k) STEM spectral image with the Ca $L_{2,3}$ edge shown in (l) for the selected area.

Rietveld refinement analysis indicated that the silicon underwent a structural transformation and was converted to a crystalline phase at the end of discharge. Both Gen F and Gen FMC samples showed excellent fitting with the reference pattern of $Li_{15}Si_4$ (JCPDS. 27-1402) as the final product with low $R_{wp}$ and chi values. Moreover, the Gen FMC sample exhibited a significant increase in lattice parameters from 10.725 to 10.7282 compared to Gen F, which suggests the intercalation of multivalent ions from the electrolyte into the Si lattice during the lithiation process. The insertion of multivalent ions from the electrolyte into the bulk Si can cause lattice expansion, as the intercalated ions occupy interstitial sites within the Si lattice. The observed increase in the lattice parameter in the Gen FMC sample provides further evidence for the intercalation of Mg and Ca ions into the $Li_{15}Si_4$ compound. In the Gen FMC sample, it was observed that Mg and Ca ions potentially occupy the Li 2 site in the lithium silicide, forming a $Li_{14.502}M_{0.498}Si_4$ quaternary Zintl phase (M: Mg and Ca), as confirmed by XRD peak fitting with the crystalline information on $Li_{15}Si_4$. To investigate the influence of the mixed-salt electrolyte on the formation of the Zintl phase, HRXRD analysis was performed on Gen FC, which served as a single-salt electrolyte with the same total concentration as the mixed salt, at the end of the discharge process under the same conditions. Figure S8 clearly illustrates a close match between Gen FC and $Li_{15}Si_4$ (JCPDS. 27-1402). Notably, Ca ions occupying the Li 2 site of lithium silicide resulted in a composition of $Li_{14.823}Ca_{0.177}Si_4$, forming a ternary Zintl phase. By considering the results obtained from refinement and the values of the multivalent ions inserted

into the Zintl phase, it can be inferred that the mixed-salt electrolyte allows inserting higher amounts of multivalent ions into $Li_{15}Si_4$ compared to when using a single-salt electrolyte.[24] In the previous report, it has been shown that ternary Zintl phases enhance the lithiation/stability and decrease the specific impedance of the negative electrolyte, leading to a significant improvement in cycling performance.[20] In terms of structure stability, the multivalent Mg and Ca ion insertion lithium silicide has been found to increase the thermodynamic stability by formation of the Li−M−Si quaternary Zintl phase, playing a crucial role in improving the electrochemical performance and stability of the Gen FMC cell, as evident from the results presented in Figures 1 and S6.

**3.3. SEI Composition and Morphology after Cycling and Calendar Aging.** To understand the morphology and composition of the SEI layer on the Si surface, Cryo STEM was conducted after extended cycling and calendar life tests. Figure 4 shows EELS and EDS mapping of Gen F and Gen FMC after 100 cycles. During 100 cycles, the Si particles in the Gen F electrolyte lost their morphology and became more pulverized compared with the Si particles in the Gen FMC electrolyte. This can be attributed to the stable SEI which can restrain dendrite growth and surface roughening and reduce the unexpected side reactions at the SEI/electrolyte interface, as depicted in Figure 4a,f.[35] The $SiO_2$ formed due to the oxidation of Si was visualized by mapping the signal from the Si and $SiO_2$ components, which was measured by analyzing the Si $L_{2,3}$ edge (Figure 4b,g). Si particles in both Gen F and Gen FMC cells were found to be encased in a thin layer of $SiO_2$, suggesting a chemical transformation of Si to $SiO_2$ at the particle edges. Specifically, the Gen F particles exhibited a higher $SiO_2$ signal on the surface. The chemical transformation from Si to $SiO_2$ directly contributes to electrochemical capacity fade and performance degradation.[36] Figure 4c,h demonstrate Li EELS analysis confirming the presence of Li within the SEI layer. Notably, for Si particles with a Gen F electrolyte, it was observed that Li covered the Si surface more extensively, suggesting a higher concentration of trapped Li in the Gen F sample. NMR experiments performed in similar samples also aligned well with this observation. In contrast, for Si particles with Gen FMC electrolyte, the Li layer was relatively evenly distributed around the particle, indicating a more uniform SEI formation. Figure 4d also confirmed that the Gen F sample has a thicker surface layer than the Gen FMC sample.

After calendar life tests, where samples were kept at voltage holds, EELS analysis and EDS elemental maps were conducted for the Si anode with Gen F and Gen FMC electrolyte to observe the built-up SEI layer as shown in Figure 5, S9, and S10. EDS mapping images of Gen F and Gen FMC electrolytes revealed that the SEI layer formed on Si particles after calendar life test was more uniform and present in lesser amounts compared to the SEI layer formed after 100 cycles. The SEI layer seems to penetrate deeper into the Si particles after cycling (Figure 4), whereas after the calendar life test, it was mostly confined to the surface. Moreover, the SEI composition can be deduced from element-by-element mapping analysis. For Gen FMC electrolyte, the distribution of Ca element on the surface is more prominent compared to the Mg element. The mapping image suggests that Ca, F, and O elements are highly concentrated along the surface. By integrating the EELS and EDS mapping results, it is suggested that the SEI layer formed by Gen FMC likely comprises Ca, Mg, F, O, and Li species. The corresponding TEM image and chemical component mapping of Si, $SiO_2$, and Li are provided in Figure 5i,j. Uniform SEI layer which included Li element surrounded on Si surface with around 10 nm thickness. Figure 5l shows the Ca $L_{2,3}$-edge EELs spectra of the Si particle at the edge region with Gen FMC (yellow box region in Figure 5k). The observed two sharp peaks in the spectra were due to the splitting of the Ca 2p state into $2p_{2/3}$ (L3) and $2p_{1/3}$ (L2),[37] located at approximately 349 and 353 eV, respectively. EELS analysis revealed that the Ca edge EELS signals of the Si with Gen FMC electrolyte closely matched those of $CaF_2$ at around 349 eV.[38] This similarity in the EELS signals indicates the presence of Ca species, particularly $CaF_2$, within the SEI layer formed on the Si surface.

Multinuclear solid-state NMR experiments were performed on cycled and voltage hold samples to explore the effect of multivalent cations on SEI layer composition and their differences after cycling versus voltage hold. Consistent with the STEM results, $^{19}F$ MAS NMR data of the samples show significant $CaF_2$ formation for the Gen FMC samples (Figure 6). This build up is more pronounced for voltage hold samples,

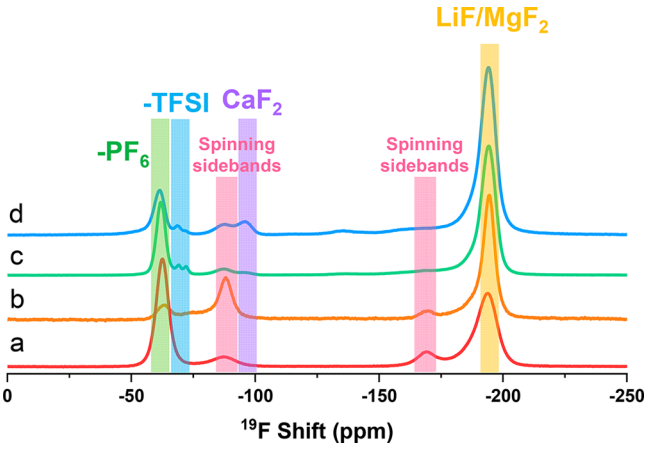


**Figure 6.** $^{19}F$ MAS NMR: Gen F after (a) cycle life and (b) calendar life with voltage hold; Gen FMC after (c) cycle life and (d) calendar life with voltage hold.

suggesting that the presence of $CaF_2$ helps protect the silicon surface from side reactions. Comparison of the data for cycled and voltage hold samples reveals that more electrolyte and salt are consumed, forming more metal fluorides, during voltage hold as opposed to continuous cycling. Although the $^{19}F$ NMR peak positions for LiF and $MgF_2$ species are close and can overlap with each other, the lack of obvious peak broadening/shoulder formation in the −200 ppm region for Gen FMC samples suggest that $CaF_2$ formation is more dominant after both cycling and voltage hold and $Mg^{2+}$ cations are diffused into the bulk forming the quaternary Li−M−Si Zintl phase. $^{19}F$ NMR data on the single salt (either $Mg(TFSI)_2$ or $Ca(TFSI)_2$) voltage hold samples show that the presence of different multivalent cations alter the LiF content formed on the surface (Figure S11). When only $Mg(TFSI)_2$ is used, more $MgF_2$ is formed with less LiF on the surface. When only $Ca(TFSI)_2$ is used, $^{19}F$ NMR data show relatively more LiF on the surface and the presence of $CaF_2$ provides a more robust and a dense SEI protecting silicon surface.[21]

Figure 7 shows $^{1}H/^{13}C$ cross-polarization MAS NMR data of silicon anodes after cycling and voltage hold with Gen F and Gen FMC electrolytes, providing insights on carbon-bearing

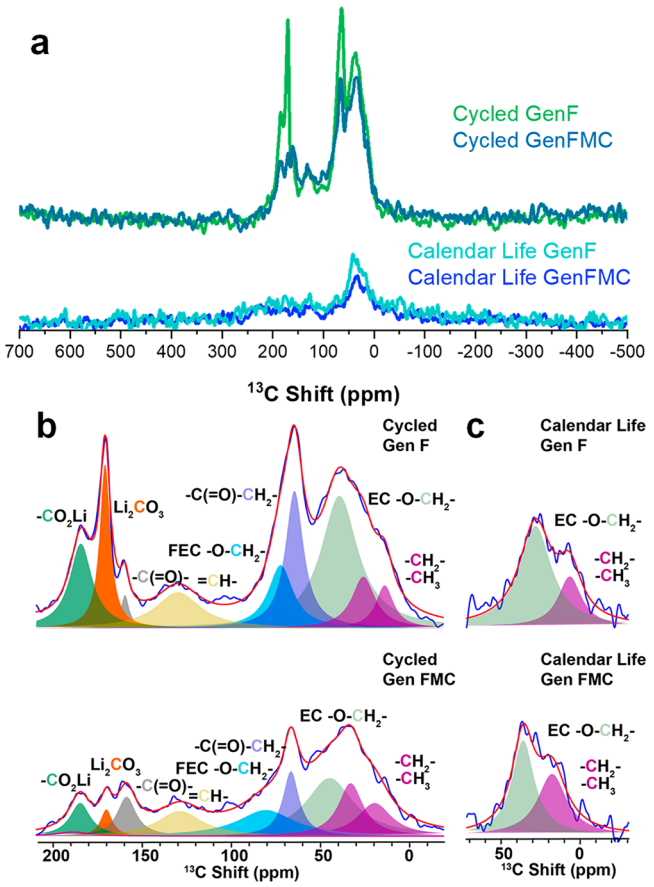


**Figure 7.** $^{1}H/^{13}C$ cross-polarization MAS NMR data of the Si anode (a) after cycling and voltage hold. Expanded plots of NMR data (b) after cycling between −10 and 200 ppm and (c) after voltage hold between −30 and 70 ppm.

species on the silicon anode surface. Comparing the cycled samples with the ones after voltage hold, the latter show less carbon-bearing SEI buildup with only aliphatic carbons such as methyl/ethyl and ether groups with peaks within the 0−50 ppm region centering at ∼20 and ∼40 ppm, respectively, regardless of the electrolyte used. On the other hand, organic SEI layer buildup after 100 cycles seems to be higher with distribution of different $^{13}C$ peaks within the 0−200 ppm region, as shown in Figure 7a. Apart from aliphatic carbons similar to voltage hold samples, peaks at ∼70 ppm suggest the presence of trapped EC and/or $-CH_2O(CH_2-)$ and peaks within the 100−200 ppm region show the presence of EC, $ROCO_2R'$ (∼160 ppm), $Li_2CO_3$ (∼170 ppm), and $RCO_2Li$ (∼185 ppm) groups from electrolyte decomposition.[12,13] Regardless of the electrolyte used, samples after cycling show $^{13}C$ peaks in the 120−140 ppm region for −CH=CH− species. These obvious differences between the presence of additional carbon bearing species and peak intensities between the two set of samples show that a thicker SEI, further decomposition of the electrolyte, and higher surface buildup for cycled samples with respect to voltage hold electrodes, consistent with the microscopy results discussed earlier. The effect of multivalent cations on SEI composition and electrochemical performance can be analyzed by comparing the $^{1}H/^{13}C$ CP NMR data for electrodes cycled in Gen F and Gen FMC (Figure 7b). The former shows larger peak areas for $Li_2CO_3$, lithium carboxylate, and trapped EC (peaks at ∼10, ∼185, and ∼70 ppm), exhibiting a greater amount of lithium-bearing SEI and could be contributing to lithium trapping and loss affecting the cycle performance. Relative intensity comparisons of $^{7}Li$ MAS NMR data of the same samples are also consistent with this observation (Figure S12).

The changes in silicon environments before and after cycling and voltage hold were also studied with $^{29}Si$ MAS NMR. As shown in Figure S13, pristine silicon has distribution of different silicon environments, including crystalline silicon (−80 ppm), amorphous silicon (−60 ppm), silicon oxide (−100 ppm), and silicon−carbon species (−20 ppm) due to surface coating. Because of the relaxation difference of each different silicon environment, multiple pulse sequences with different pulse delays were applied to capture all the silicon environments quantitatively, both in bulk and on the surface. The details of these experiments are explained in the Supporting Information. The changes in bulk silicon with cycling and voltage hold were studied with $^{29}Si$ direct polarization and spin-echo NMR experiments and compared with the pristine electrode data, which is discussed in the Supporting Information. After cycling and voltage hold, crystalline silicon environments mostly disappeared, and samples show mostly silicon oxide as bulk silicon environment, consistent with the TEM data discussed earlier. The changes in silicon surface and SEI composition were also studied via $^{1}H/^{29}Si$ cross-polarization (CP) NMR after 100 cycles and one month voltage hold (Figure 8). The experiment specifically enhances the silicon environments in the vicinity of protons and therefore emphasizes surface silicon providing insights on SEI composition. Similar to $^{1}H/^{13}C$ CP NMR data, the major differences between the cycled and voltage hold sample is the amount and type of silicon-bearing SEI buildup. The latter shows mostly hydroxyl terminated silicate environments with major peak at the ∼−100 ppm region and with less peak intensities, indicating less SEI buildup in terms of quantity and diversity. Whereas the cycled samples show additional peaks at ∼90, −70, −60, −40, −20, and 0 ppm region. These peaks can be tentatively assigned as hydroxyl terminated silicates ($Q^2$ and $Q^1$), $Q^0$ silicates coordinated to Li, lithium silicates/$T^3$ organosiloxanes, amorphous silicon, and alkysilanes, respectively.[39] These assignments suggest that surface silicon oxides and hydroxides are reduced to form organasiloxenes and that silicon interphase is bonded to the organic SEI. The relative peak intensity comparison of GenF and GenFMC samples suggests that $SiOx/H_x$ reduction is more pronounced for GenF than the GenFMC sample, after cycling.

The outcomes of these characterization studies show that the use of mixed multivalent cations not only affects SEI composition and morphology in comparison to baseline electrolyte but also provides enhanced cation insertion into the bulk forming stable quaternary Li−M−Si Zintl phases. The diverse inorganic SEI layer with a mixture of LiF, $CaF_2$, and $MgF_2$ improves the mechanical properties, interfacial stability, and ion transport capabilities, providing a better protective layer. The formation of the Li−Ca/Mg−Si quaternary Zintl phase partially mitigates the high reactivity issue of lithium silicides inhibiting further reaction with the electrolyte and binder during electrochemical cycling and holds. NMR characterization data suggest that the organic SEI layer formed with multivalent electrolytes has less lithium bearing managing lithium loss. The benefits of using a mixed salt of Mg and Ca cation originates from their differences in cation size, oxide and

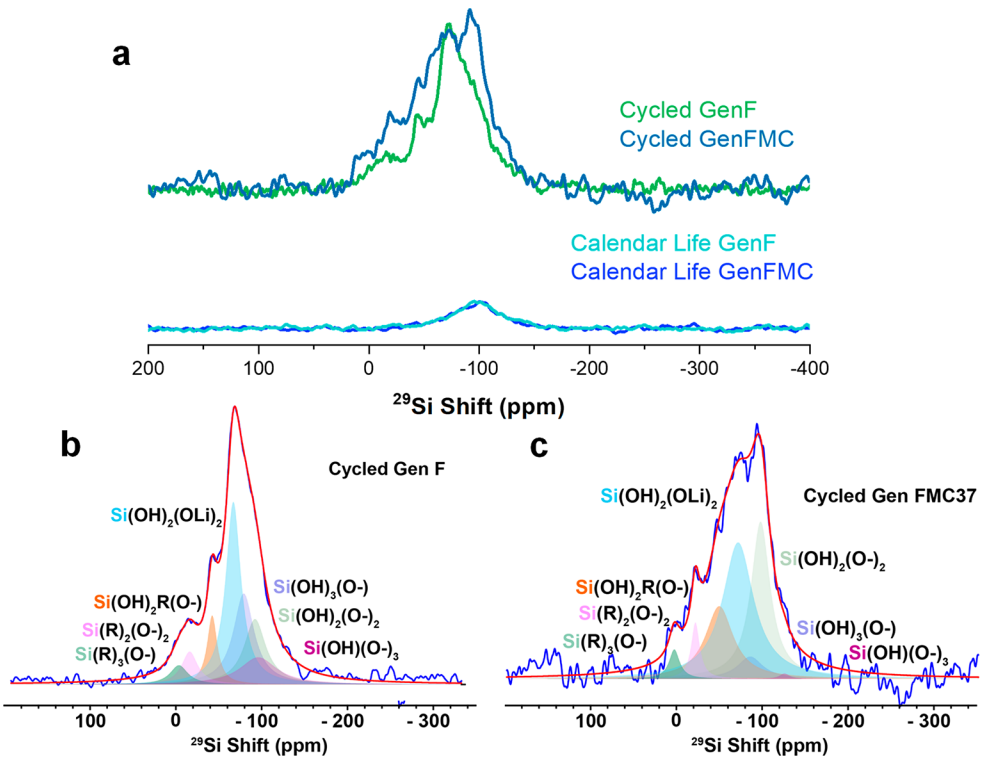


**Figure 8.** (a) $^{1}H/^{29}Si$ cross-polarization MAS NMR data of the Si anode after cycling and voltage hold. Expanded plots of NMR data after cycling for (b) baseline and (c) additive samples.

fluoride formation energies[21] and diffusion into the bulk altering both silicon surface and bulk simultaneously.

## 4. CONCLUSION

This work shows the benefits of using mixed salts of $Ca(TFSI)_2$ and $Mg(TFSI)_2$ as electrolyte additives for Si anodes. The formation of ternary Zintl phases and modification of the silicon SEI layer with $CaF_2$ formation had been previously shown to improve silicon calendar life and cycling performance by our previous studies. However, in this study, we formulated a specific additive combination, a mixture of $Mg(TFSI)_2$ and $Ca(TFSI)_2$ with a specific ratio with which not only the multivalent cation insertion into the bulk is enhanced but also the composition of the silicon interface is altered, protecting both surface and bulk silicon.

Structure refinement study reveals that mixed-salt additives promote the formation of crystalline Li−M−Si phases by the co-insertion of Mg and Ca, which is critical in enhancing the bulk stability, reducing the bulk resistance of the anode, and ultimately improving the electrochemical performance of the battery. In terms of surface stabilization, our findings supported by Cryo-STEM and NMR analysis, suggest that multivalent salts are advantageous for building a stable SEI layer compared to Gen F and that a stable SEI layer can be achieved through the formation of $CaF_2$ and stable organic layers with less Li-containing carbonates and carboxylates, resulting in less Li consumption. The simultaneous stabilization of the bulk and surface of Si anodes through mixed-salt additives results in improved calendar life performance, higher specific capacity, and better Coulombic efficiency of the full cell compared to the baseline electrolyte. The study proves that with accurate control of the electrolyte formulation, it can be customized to accommodate a range of silicon materials, making it a practical choice for anodes in commercial products, including but not limited to electric vehicles, portable electronics, and renewable energy storage systems. These results contribute to the ongoing efforts to develop more efficient and reliable energy storage systems with a higher energy density and improved lifetime for a wide range of applications.

## ■ ASSOCIATED CONTENT

### Supporting Information

Electrochemical performance (cycle and calendar life performance), ex situ SEM image after cycle and calendar life test, EIS fitting results, Rietveld refinement pattern, EDS mapping and STEM image, $^{7}Li$ MAS NMR and $^{29}Si$ NMR of calendar and cycle life test sample (PDF)

## ■ AUTHOR INFORMATION


### Corresponding Author

**Fulya Dogan** − *Chemical Sciences and Engineering Division, Argonne National Laboratory, Lemont, Illinois 60439, United States;* orcid.org/0000-0001-7997-266X; Email: fdogan@anl.gov

### Authors

**Sohyun Park** − *Chemical Sciences and Engineering Division, Argonne National Laboratory, Lemont, Illinois 60439, United States;* orcid.org/0000-0002-3641-1202

**Haoyu Liu** − *Chemical Sciences and Engineering Division, Argonne National Laboratory, Lemont, Illinois 60439, United States*

**Joseph Quinn** − *Energy and Environment Directorate, Pacific Northwest National Laboratory, Richland, Washington 99354, United States*
**Saul H. Lapidus** − *X-ray Science Division, Advanced Photon Source, Argonne National Laboratory, Lemont, Illinois 60439, United States;* orcid.org/0000-0002-7486-4325
**Yunya Zhang** − *Chemical Sciences and Engineering Division, Argonne National Laboratory, Lemont, Illinois 60439, United States;* orcid.org/0000-0002-9411-0184
**Stephen E. Trask** − *Chemical Sciences and Engineering Division, Argonne National Laboratory, Lemont, Illinois 60439, United States;* orcid.org/0000-0002-0879-4779
**Chongmin Wang** − *Energy and Environment Directorate, Pacific Northwest National Laboratory, Richland, Washington 99354, United States;* orcid.org/0000-0003-3327-0958
**Baris Key** − *Chemical Sciences and Engineering Division, Argonne National Laboratory, Lemont, Illinois 60439, United States;* orcid.org/0000-0002-1987-1629

### Author Contributions

The manuscript was written through contributions of all authors. All authors have given approval to the final version of the manuscript.

### Funding

U.S. Department of Energy, Office of Vehicle Technologies Contract No. DE-AC02-06CH11357.

### Notes

The authors declare no competing financial interest.

## ■ ACKNOWLEDGMENTS

The authors would like to thank Brian Cunningham and David Howell from the Office of Vehicle Technologies, at the U.S. Department of Energy, Office of Energy Efficiency and Renewable Energy for their Silicon Consortium Project support. The work at Argonne National Laboratory was supported by the U.S. Department of Energy, Office of Vehicle Technologies. The submitted manuscript has been created by UChicago Argonne, LLC, Operator of Argonne National Laboratory ("Argonne") a U.S. Department of Energy Office of Science laboratory, operated under Contract No. DE-AC02-06CH11357. Part of the TEM work was carried out at the William R. Wiley Environmental Molecular Sciences Laboratory, a national scientific user facility sponsored by U.S. Department of Energy, Office of Biological and Environmental Research and located at PNNL. PNNL is operated by Battelle for the U.S. Department of Energy under contract DE-AC05-76RL01830.

## ■ REFERENCES

(1) Braun, P. V.; Cho, J.; Pikul, J. H.; King, W. P.; Zhang, H. High power rechargeable batteries. *CURR Opin Solid St M* **2012**, *16*, 186−198.
(2) Park, S.; et al. A new material discovery platform of stable layered oxide cathodes for K-ion batteries. *Energy Environ. Sci.* **2021**, *14*, 5864−5874.
(3) Liu, X.; et al. Designing advanced electrolytes for lithium secondary batteries based on the coordination number rule. *ACS Energy Lett.* **2021**, *6*, 4282−4290.
(4) Cano, Z. P.; et al. Batteries and fuel cells for emerging electric vehicle markets. *Nat. Energy* **2018**, *3*, 279−289.
(5) Gaines, L.; Nelson, P. In *13th International Battery Materials Recycling Seminar and Exhibit*; Broward County Convention Center, Fort Lauderdale, FL; 16.
(6) Zhang, L.; et al. Lithium lanthanum titanate perovskite as an anode for lithium ion batteries. *Nat. Commun.* **2020**, *11*, 3490.
(7) Zhang, H.; Yang, Y.; Ren, D.; Wang, L.; He, X. Graphite as anode materials: Fundamental mechanism, recent progress and advances. *Energy Storage Mater.* **2021**, *36*, 147−170.
(8) Lee, P. K.; Tahmasebi, M. H.; Ran, S.; Boles, S. T.; Yu, D. Y. Leveraging Titanium to Enable Silicon Anodes in Lithium-Ion Batteries. *Small* **2018**, *14*, 1802051.
(9) Han, B.; et al. Spontaneous repairing liquid metal/Si nanocomposite as a smart conductive-additive-free anode for lithium-ion battery. *Nano Energy* **2018**, *50*, 359−366.
(10) Cangaz, S.; et al. Enabling High-Energy Solid-State Batteries with Stable Anode Interphase by the Use of Columnar Silicon Anodes. *Adv. Energy Mater.* **2020**, *10*, 2001320.
(11) Rahman, M. A.; Song, G.; Bhatt, A. I.; Wong, Y. C.; Wen, C. Nanostructured silicon anodes for high-performance lithium-ion batteries. *Adv. Funct. Mater.* **2016**, *26*, 647−678.
(12) Obrovac, M.; Krause, L. Reversible cycling of crystalline silicon powder. *J. Electrochem. Soc.* **2007**, *154*, A103.
(13) Richter, K. *Film formation, side reactions and interactions in Si/C negative electrodes in Lithium ion batteries*; Universität Ulm, 2020.
(14) Key, B.; et al. Real-time NMR investigations of structural changes in silicon electrodes for lithium-ion batteries. *J. Am. Chem. Soc.* **2009**, *131*, 9239−9249.
(15) Key, B.; Morcrette, M.; Tarascon, J.-M.; Grey, C. P. Pair distribution function analysis and solid state NMR studies of silicon electrodes for lithium ion batteries: understanding the (de) lithiation mechanisms. *J. Am. Chem. Soc.* **2011**, *133*, 503−512.
(16) Nesper, R.; Von Schnering, H.; Curda, J. Li12Si7, a Compound with Trigonal Planar Si4 Clusters and Isometric Si5 Rings. *Chem. Ber.* **1986**, *119*, 3576−3590.
(17) Wu, H.; Cui, Y. Designing nanostructured Si anodes for high energy lithium ion batteries. *Nano Today* **2012**, *7*, 414−429.
(18) Szczech, J. R.; Jin, S. Nanostructured silicon for high capacity lithium battery anodes. *Energy Environ. Sci.* **2011**, *4*, 56−72.
(19) Krupp, A.; et al. Calendar aging model for lithium-ion batteries considering the influence of cell characterization. *J. Energy Storage* **2022**, *45*, 103506.
(20) Li, X.; et al. Investigating Ternary Li−Mg−Si Zintl Phase Formation and Evolution for Si Anodes in Li-Ion Batteries with Mg(TFSI)2 Electrolyte Additive. *Chem. Mater.* **2021**, *33*, 4960−4970.
(21) Zhang, Y.; et al. Silicon anodes with improved calendar life enabled by multivalent additives. *Adv. Energy Mater.* **2021**, *11*, doi.
(22) Kalaga, K.; Rodrigues, M.-T. F.; Trask, S. E.; Shkrob, I. A.; Abraham, D. P. Calendar-life versus cycle-life aging of lithium-ion cells with silicon-graphite composite electrodes. *Electrochim. Acta* **2018**, *280*, 221−228.
(23) Han, B.; et al. Using mixed salt electrolytes to stabilize silicon anodes for lithium-ion batteries via in situ formation of Li−M−Si ternaries (M = Mg, Zn, Al, Ca). *ACS Appl. Mater. Interfaces* **2019**, *11*, 29780.
(24) Uppuluri, R.; et al. Electrochemical Formation of Li-M-(M′)-Si Phases Using Multivalent Electrolyte Salt Additives. *J. Electrochem. Soc.* **2023**, *170*, 030501.
(25) Araño, K. G.; et al. Functionalized Silicon Particles for Enhanced Half- and Full-Cell Cycling of Si-Based Li-Ion Batteries. *ACS Appl. Mater. Interfaces.* **2023**, *15*, 10554−10569.
(26) Broussely, M.; et al. Aging mechanism in Li ion cells and calendar life predictions. *J. Power Sources* **2001**, *97*−*98*, 13−21.
(27) Lu, B.; Ning, C.; Shi, D.; Zhao, Y.; Zhang, J. Review on electrode-level fracture in lithium-ion batteries. *Chin. Phys. B* **2020**, *29*, 026201.
(28) An, S. J.; et al. The state of understanding of the lithium-ion-battery graphite solid electrolyte interphase (SEI) and its relationship to formation cycling. *Carbon* **2016**, *105*, 52−76.

(29) Portet, C.; Taberna, P. L.; Simon, P.; Flahaut, E. Influence of carbon nanotubes addition on carbon−carbon supercapacitor performances in organic electrolyte. *J. Power Sources* **2005**, *139*, 371−378.
(30) Saidani, F.; Hutter, F. X.; Scurtu, R. G.; Braunwarth, W.; Burghartz, J. N. Lithium-ion battery models: a comparative study and a model-based powerline communication. *Adv. Radio Sci.* **2017**, *15*, 83−91.
(31) Zhang, S. S.; Xu, K.; Jow, T. R. EIS study on the formation of solid electrolyte interface in Li-ion battery. *Electrochim. Acta* **2006**, *51*, 1636−1640.
(32) Park, S.; et al. C-$Na_3V_{1.96}Fe_{0.04}(PO_4)_3/Fe_2P$ nanoclusters with stable charge-transfer interface for high-power sodium ion batteries. *J. Chem. Eng.* **2021**, *404*, 126974.
(33) Zaban, A.; Zinigrad, E.; Aurbach, D. Impedance Spectroscopy of Li Electrodes. 4. A General Simple Model of the Li−Solution Interphase in Polar Aprotic Systems. *J. Phys. Chem.* **1996**, *100*, 3089−3101.
(34) Choi, W.; Shin, H.-C.; Kim, J. M.; Choi, J.-Y.; Yoon, W.-S. Modeling and Applications of Electrochemical Impedance Spectroscopy (EIS) for Lithium-ion Batteries. *J. Electrochem. Sci. Technol.* **2020**, *11*, 1−13.
(35) Wang, A.; Kadam, S.; Li, H.; Shi, S.; Qi, Y. Review on modeling of the anode solid electrolyte interphase (SEI) for lithium-ion batteries. *Comput. Mater.* **2018**, *4*, 15.
(36) Quinn, J.; et al. Tracking the Oxidation of Silicon Anodes Using Cryo-EELS upon Battery Cycling. *ACS Nano* **2022**, *16*, 21063−21070.
(37) Rossi, A. L.; et al. Effect of strontium ranelate on bone mineral: analysis of nanoscale compositional changes. *Micron* **2014**, *56*, 29−36.
(38) Jiang, N. Local order of Ca in a $CaF_2-Al_2O_3-SiO_2$ glass by electron energy-loss spectroscopy. *J. Appl. Phys.* **2011**, *110*, 013518.
(39) Rim, G.; Marchese, A. K.; Stallworth, P.; Greenbaum, S. G.; Park, A.-H. A. $^{29}Si$ solid state MAS NMR study on leaching behaviors and chemical stability of different Mg-silicate structures for $CO_2$ sequestration. *J. Chem. Eng.* **2020**, *396*, 125204.